**Jennifer Coyne Albrecht**[1]
**Matthew B. Kerby**[2]
**Thomas P. Niedringhaus**[1]
**Jennifer S. Lin**[2]
**Xiaoxiao Wang**[2]
**Annelise E. Barron**[1,2]

[1]Department of Chemical Engineering, Stanford University, Stanford, CA, USA
[2]Department of Bioengineering, Stanford University, Stanford, CA, USA

Received October 29, 2010
Revised December 10, 2010
Accepted January 3, 2011

Research Article

# Free-solution electrophoretic separations of DNA–drag-tag conjugates on glass microchips with no polymer network and no loss of resolution at increased electric field strength

Here, we demonstrate the potential for high-resolution electrophoretic separations of ssDNA–protein conjugates in borosilicate glass microfluidic chips, with no sieving media and excellent repeatability. Using polynucleotides of two different lengths conjugated to moderately cationic protein polymer drag-tags, we measured separation efficiency as a function of applied electric field. In excellent agreement with prior theoretical predictions of Slater et al., resolution is found to remain constant as applied field is increased up to 700 V/cm, the highest field we were able to apply. This remarkable result illustrates the fundamentally different physical limitations of free-solution conjugate electrophoresis (FSCE)-based DNA separations relative to matrix-based DNA electrophoresis. ssDNA separations in ''gels'' have always shown rapidly declining resolution as the field strength is increased; this is especially true for ssDNA $>$ 400 bases in length. FSCE's ability to decouple DNA peak resolution from applied electric field suggests the future possibility of ultra-rapid FSCE sequencing on chips. We investigated sources of peak broadening for FSCE separations on borosilicate glass microchips, using six different protein polymer drag-tags. For drag-tags with four or more positive charges, electrostatic and adsorptive interactions with poly(*N*-hydroxyethylacrylamide)-coated microchannel walls led to appreciable band-broadening, while much sharper peaks were seen for bioconjugates with nearly charge-neutral protein drag-tags.

**Keywords:**
Band broadening / Drag-tag / End-labeled free-solution electrophoresis / Free-solution conjugate electrophoresis / Free-solution microchip electrophoresis
DOI 10.1002/elps.201000574

## 1 Introduction

Much of the DNA sequencing for the Human Genome Project was done by capillary array electrophoresis using gel-like sieving media to enable DNA size-separation [1, 2]. CE sequencing averages read-lengths of 600–750 bases of DNA per capillary in approximately 1 h [3], which is aided by automation, specifically by the use of replaceable polymer sieving matrices that are loaded and unloaded from arrays at high pressure. The development of a planar glass substrate for a miniaturized separation was a more recent advance in electrophoresis technology [4, 5]. Separation channels on microfluidic devices are typically much shorter than capillaries; thus, higher electric field strengths can be applied, allowing faster and more efficient separations. The typical cross-channel injection geometry on microchips produces a narrow injection zone, significantly decreasing the separation length necessary to achieve high-resolution DNA sequencing. CE injection plugs are on the order of 1 mm or wider, while microchip geometry-defined injection zones are typically on the order of 100 μm wide [6].

In addition to offering faster DNA separations, potentially with tinier sample aliquots, microchips offer other advantages over capillaries. In principle, the degree of

**Correspondence:** Professor Annelise E. Barron, Stanford University, 318 Campus Drive, W300B James H. Clark Center, Stanford, CA 94305-5444, USA
**E-mail:** aebarron@stanford.edu
**Fax:** +1-650-723-9801

**Abbreviations: FSCE,** free-solution conjugate electrophoresis; **HVPS,** high voltage power supply; **pHEA,** poly(*N*-hydroxyethylacrylamide); **SBE,** single-base extension; **sulfo-SMCC,** sulfosuccinimidyl 4-*N*-maleimidomethyl cyclohexane-1-carboxylate

**Colour Online:** See the article online to view Fig. 1 in colour.

 

parallelization can be increased without adding much to fabrication costs; devices can be fabricated out of glass or plastic; and a possibility exists to integrate front-end DNA sample preparation, creating ''lab-on-a-chip'' devices. High-throughput analysis on a microfluidic chip with 384 separation channels was achieved with a novel rotary fluorescence detector to collect data simultaneously in all channels [7]. Devices have been fabricated from PMMA [8, 9], polycarbonate (PC) [10, 11], and PDMS [12, 13] instead of glass. Much work has been done to create microscale total analytical systems (μTAS) that integrate sample amplification, preparation and detection into one device. For example, devices with the potential for ''sample-in/answer-out'' capabilities could be used to screen whole blood for pathogens (in $<30$ min) or to achieve human identification from both blood and buccal samples [14–16]. Integrated Sanger cycling, DNA purification and electrophoretic sequencing with a read length of 556 bases on a single microfluidic device has been demonstrated by the Mathies lab of Berkeley [17].

A significant effort was made, especially in the Barron lab, to develop ideal sieving media for electrophoretic DNA sequencing on microchips. While certain sieving media that were created and optimized for CE sequencing can work for microchip separations, polymers developed specifically for microchips achieve significantly longer read lengths. For example, high-molar mass poly(*N*-dimethylacrylamide) (pDMA) media, used with a particular wall coating, gave longer sequencing reads on glass microchips than either ABI POP$^{TM}$ [6] or the Beckman LongRead$^{TM}$ [18] matrix in the same chips. The optimized poly(*N*-dimethylacrylamide) matrix gave 600-base reads in under 6.5 min; this is ten-fold faster than CE and at least a two-thirds reduction in separation time over prior chip-based DNA sequencing [18]. The Barron lab has also developed a poly(*N*-hydroxyethylacrylamide) (pHEA) dynamic coating for microchip electrophoresis separations that almost completely suppresses EOF [19]. However, the development of highly parallel, automated DNA sequencing platform based on microfluidic devices is hampered by the necessity of high pressures to load viscous polymer networks (even media of more moderate viscosity) into microfluidic devices.

Eliminating the need for sieving media would facilitate the development of automated microchip-based DNA sequencing and ''lab-on-a-chip'' genetic analysis devices. The method of free-solution conjugate electrophoresis (FSCE) for ssDNA sequencing and sizing has been under development since 1999 [20–25]. FSCE achieves size-based electrophoretic separations of DNA without a polymer network through the use of a large, monodisperse, essentially charge-neutral ''drag-tag'' as an appendage to the end of each ssDNA molecule, to break the free-draining properties of DNA. Initial hurdles to produce an extremely pure, protein-based drag-tag were recently overcome (J. S. Lin et al., paper submitted), and the sequencing of 265 bases by CE has been demonstrated [26]. FSCE has also been applied to size-based genotyping using single-base extension (SBE) and ligase detection reaction (LDR) assays [27, 28]. With sequencing read lengths essentially on par with current next-generation sequencing technologies (but with much lower throughput and degree of parallelization), the overarching goal of this work is to create the basis for transition of FSCE separations with protein drag-tags from capillaries to microchips. Previously, the only separations by FSCE on microchips were of SBE assay products [28]. Of the 16 different drag-tags used for the SBE-FSCE separation, only one was a linear, random coil, genetically engineered protein polymer as is necessary for long-read sequencing [29]. These separations were successful, yet the peak for the protein polymer was broad with low signal intensity.

With the long-term goal of sequencing by FSCE on microchips, we detail ssDNA separations on glass microchips with monodisperse protein polymer drag-tags of six increasing lengths and/or charge. In a significant departure from polymer matrix-based separations, we show that resolution is not affected by increased electric field strength (up to 700 V/cm, the maximum possible with the high voltage power supply (HVPS) and chosen microchip). The band-broadening sources in FSCE separations were determined. Overall, this paper demonstrates the significant benefits of free-solution bioconjugate electrophoresis on microchips, providing a stronger foundation for our work toward the ultimate goal of chip-based FSCE sequencing.

## 2 Materials and methods

### 2.1 Drag-tag production

Two different methods were used to produce protein polymer drag-tags. The first was previously described in detail and was used to express and purify four proteins; the seven amino acid ''monomer'' unit GAGTGSA made up the repeating sequence of the proteins, and 1 of every 9 serines was mutated to an arginine by *Escherichia coli* (J. S. Lin et al., paper submitted). The proteins had 18, 27, 36, and 72 repeats of this sequence (141, 204, 267, and 516-aa total length, respectively). The second method used a self-cleaving intein system to achieve two ''highly'' charged protein polymers (X. Wang et al., paper submitted). One was 110-aa long with 6 arginines (''6-Arg'') and the amino acid sequence (GTAGSAGTAGSATGAGSAGSRGTAGSGATGASGTGR)$_3$-GA, and the second was 182-aa long with 12 arginines (''12-Arg'') and the sequence (GTAGSATGAGSAGSRGTAGSGATGASGTGR)$_6$-GA.

### 2.2 Coupling of protein drag-tags to ssDNA

The drag-tags were conjugated to DNA using the previously described protocol [25, 26, 28]. All DNA oligomers were purchased from IDT (Integrated DNA Technologies, Coralville, IA, USA) with a 5′-thiol modification for conjugation and either an internal or 3′-fluorescein. The sequences were 42-nt ($\mathbf{X}_1$-TGT-GGT-AGT-TGG-AGC-TGG-TGC-CGT-

 

AGG-CAA-GAG-TGC-CTT-GAC-$\mathbf{X_2}$), 44-nt ($\mathbf{X_1}$-ACT-TGT-GGT-AGT-TGG-AGC-TGG-TCG-CGT-AGG-CAA-GAG-TGC-CTT-GA-$\mathbf{X_2}$), and 74-nt ($\mathbf{X_1}$-GTT-TTC-CCA-G-$\mathbf{X_3}$-C-ACG-ACG-TTG-TAA-AAC-GAC-GGC-CAG-TGC-CAA-GCT-TGC-ATG-C CT-GCA-GGT-CGA-CTC-TAG-AGG-AT), where $\mathbf{X_1}$ = 5′-C6 thiol linker, $\mathbf{X_2}$ = 3′-fluorescein, $\mathbf{X_3}$ = internal dT-fluorescein. In the first step, the single amine of each protein is activated with the heterobifunctional linker sulfo-SMCC (sulfosuccinimidyl 4-*N*-maleimidomethyl cyclohexane-1-carboxylate, Thermo Fisher Scientific, Waltham, MA, USA) by mixing it with a 10:1 molar excess of sulfo-SMCC. The mixture is gently vortexed for 1 h and then lyophilized after removing excess sulfo-SMCC with a CentriSep gel filtration column (Princeton Separations, Adelphia, NJ, USA). Second, the thiol group of the ssDNA is reduced by incubating it with a 20-fold molar excess of TCEP (tris(2-carboxyethylphosphine), Thermo Fisher Scientific) in a 100-mM sodium phosphate buffer (pH 7.5), for 100 min at 40°C. Finally, the reduced DNA is mixed with a 100-fold molar excess of the sulfo-SMCC-activated drag-tag in sodium phosphate buffer for 4–18 h. The conjugated DNA–drag-tag samples were diluted to a 2-μM concentration prior to use.

### 2.3 Microchip electrophoresis

Electrophoresis was performed using a novel custom-built system similar to the Barron lab's previously described system [30] with updated components for highly sensitive detection of multi-color DNA fragments by laser-induced fluorescence (LIF). The system consists of a HVPS capable of rapid switching, and an optical system to detect fluorescently labeled molecules as they migrate past a chosen detection point. A single program, written in LabVIEW, controls the HVPS and optical subsystems, while simultaneously collecting data. The computer is equipped with three National Instruments data acquisition cards (NI 6722, NI 6224, NI PCIE6251). The operating program and HVPS (model HVPS-6000) were designed and developed specifically for the Barron group by Etendu (Fremont, CA, USA).

The HVPS has four electrodes that are each connected to a paired, switchable voltage unit for a total of eight independent, internal voltage sources. Voltages up to 6000 V (monopolar) can be applied independently at each electrode channel. Each channel can also be disconnected (floated) from the circuit. The applied voltage for each electrode as a function of time is controlled through an automated LabVIEW program interface, which allows implementation of multiple steps. The HVPS can switch voltages between power supplies at up to 60 Hz without voltage slew; the voltage and current data at each electrode channel are collected by the LabVIEW software during each run.

The optical system consists of a laser, inverted microscope, and charge-coupled device (CCD). A Nikon Ti-U inverted, epifluorescence microscope was fitted with a Nikon "Ti-PAU photoactivation illuminator unit 4" to connect a 40 mW Spectra-Physics Cyan$^{TM}$ Scientific CW 488-nm laser (Newport) through a single-mode fiber optic cable (QSMF-488-3.5/125-3-L, Oz Optics, Canada). From the rear of the microscope, the laser beam is channeled through a 488-nm laser line clean-up filter (LL01-488-25, Semrock) to eliminate harmonic laser wavelengths before passing through a Nikon 40 × /0.6NA-ELWD-S Plan Fluor microscope objective. The laser is focused on the center of the microfluidic channel as a 10- to 20-μm spot with ~11 mW power as measured using a Thorlabs PM120 power meter with S120 sensor. The cross-hatched pattern etched in the Micralyne chip that is set away from the separation channel (where detection occurs) provides a reference to accurately and consistently focus the laser spot at the same distance from the injection cross. When fluorescently labeled molecules migrate past the laser spot, the emitted light is collected by the objective, reflected fully, and passed through a long pass emission filter (LP02-488RU-25, Semrock). After emerging from a side port of the microscope via a 1 × C-mount adapter (Diagnostic Instruments, Sterling Heights, MI, USA), light passes through a fused silica plane transmission grating (FSTG-VIS1379, Ibsen Photonics, Denmark) to spatially separate the emitted wavelengths, which then impinge onto a back-thinned CCD (S7031-0907S, Hamamatsu, Japan). The CCD is mounted into a C7041 single-stage camera head that cools the device to −10°C for thermal noise reduction. The prism maps the emitted wavelength to a physical position on the CCD. The grating and camera are mounted to a 12 by a 6-inch aluminum breadboard fitted with adjustable optics component fixtures to align the optics pathway. The entire CCD assembly is housed in a dark, black box. To calibrate the CCD, laser line filters in the green (10LF01-515, Newport) and red (10LF01-633, Newport) wavelengths are placed over a countersunk hole in a flat, black thermoplastic sheet over the objective and illuminated with white light from the tungsten lamp of the microscope. The 515- and 633-nm line locations are marked as the lower and upper wavelength boundaries in the custom software. Linear interpolation determines the wavelength for each physically illuminated CCD position. Using a custom hardware interface, the CCD data is collected at up to 100 Hz to ensure capture of closely spaced fragments and is stored by LabVIEW. The software allows input of up to 10 wavelength ranges for data collection. For the purpose of these experiments, fluorescein dyes are used, and the data were collected in the window $\lambda$ = 510–540 nm.

Experiments were carried out on planar glass microchips with a simple-cross injection geometry (model SC, Micralyne, Canada). The chips have a 50-μm injection cross, channels that are 50 μm wide and 20 μm deep, and an 8.0 cm distance from the injection zone to the analysis waste well. The borosilicate glass microchannels were dynamically coated with a 0.3 wt% solution of pHEA to suppress EOF and some of the adsorptive interactions between the slightly positively charged protein drag-tags and the anionic walls. The coating procedure and synthesis of pHEA were

 

previously described [19]. The separation buffer was 1 × TTE (89 mM Tris, 89 mM TAPS, 2 mM EDTA) with 7 M urea. Separations were performed at 55°C using the heating plate assembly (Supporting Information Fig. S-1). Samples were injected into the separation channel by grounding the sample well and applying 350 V to the sample waste well for 40 s to electrophorese the analytes across the separation channel while the other electrodes were floated. Separation started when the voltage was rapidly switched; the analysis buffer well was grounded while voltages of 1700–5950 V (electric field strength $E = 200$–$700$ V/cm) were sequentially applied at the analysis waste well. A ''pullback'' voltage of 25 V/cm less than $E$ was applied at both the sample and sample waste wells for the duration of the separation.

## 3 Results and discussion

### 3.1 Free-solution electrophoretic separations on glass microchips

As stated above, the only previous microchip FSCE separations with a protein polymer drag-tag (18 repeats of the ''monomer'' GAGTGSA) gave a broad peak with low fluorescent signal intensity relative to the noise [28]. Here, free-solution electrophoretic injections and separations of DNA coupled to protein polymer drag-tags in glass microchips were optimized to achieve increased signal. First, buffer concentration was increased from 0.5 × to 1 × TTE (89 mM Tris, 89 mM TAPS, 2 mM EDTA) with 7 M urea [28]. The 1 × buffer concentration is consistent with FSCE separations in capillaries, and the hydrodynamic drag of a protein also increases with ionic strength [25, 26]. No peak degradation was seen with the ionic strength increase; thus, it is assumed that Joule heating can be neglected as a source of band broadening at these conditions as in capillary separations. Second, separations were performed at 55°C with a new copper heating plate and Teflon™ microchip caddy assembly (Supporting Information Fig. S-1), which increased the volume of the wells from 4 to 100 μL, eliminating previous problems with buffer evaporation and urea crystallization at 55°C. The assembly is designed to fit onto the microscope stage of the microchip electrophoresis system, and it enabled multiple runs to be performed in series without buffer ion depletion. Third, FSCE separations were performed on chips with a simple-cross injection zone geometry instead of an offset-T. This reduces the volume of the sample plug, achieving a narrower injection plug and mostly symmetric Gaussian-shaped peaks without peak tailing. Last, the ''pullback'' voltage was applied to the sample and sample waste wells for the duration of the separation instead of just the first 40 s to further reduce peak tailing. Using this optimized injection scheme, separations of DNA–drag-tag conjugates were achieved on commercially available glass microchips with protein polymer drag-tags. A representative electropherogram shows a clean separation with good signal intensity and sharp, Gaussian-like peaks when using a protein polymer drag-tag (Supporting Information Fig. S-2).

### 3.2 Duplex separation at increasing electric field strength

With an optimized microchip injection protocol, separation efficiency was tested. To evaluate the efficiency of FSCE separations on pHEA-coated glass microchips, two lengths of ssDNA (42 and 44 nt) were conjugated to the smallest protein polymer drag-tag (18-mer, 141-aa), mixed together, and separated by free-solution microchip electrophoresis. The duplex sample was separated first at an electric field strength of $E = 300$ V/cm, which is similar to the $E = 310$ V/cm used for CE separations. The sample was then separated at increasing $E$ up to 700 V/cm (the upper limit of the HVPS, $E$ was increased in increments of 50 V/cm). The duplex separations are shown in Fig. 1.

The first peak to elute is excess ''free'' unconjugated DNA, and the pair of peaks eluting later are the 44- and 42-nt DNA molecules coupled to the 18-mer drag-tag. The bioconjugate peaks for both the 44- and 42-nt oligomers are clearly resolved at every condition tested. The resolution between the two conjugate peaks was calculated using the

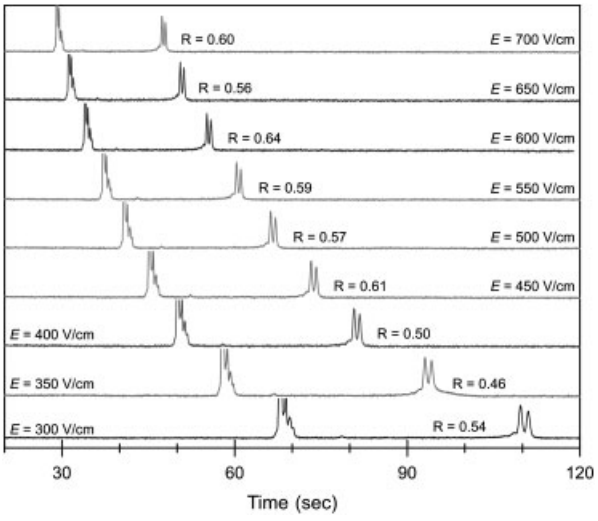


**Figure 1.** Microchip electrophoresis of a mixture of two DNA oligomers (42- and 44-nt) conjugated to the 18-mer (141-aa) drag-tag, separated at increasing $E$. Sample was separated by free-solution electrophoresis in 1 × TTE buffer with 7 M urea, at 55°C in a Micralyne SC glass chip coated with pHEA for EOF suppression. The sample was electrophoresed from the sample to sample waste well at 350 V/cm for 40 s before the electric field was switched and applied along the length of the separation channel at the noted electric field strengths. ''Pullback'' voltages were applied to sample and sample waste wells of an equivalent of 25 V/cm less than $E$. Detection occurred at $L = 7.2$ cm from the injection zone. Resolution of the pair of peaks is shown on the electropherogram.

 

following equation [31]:

$$R = \frac{\sqrt{2 \cdot \ln 2} \cdot (T_2 - T_1)}{(W_2 + W_1) \cdot (M_2 - M_1)} \quad (1)$$

where $T$ is the migration time of the center of the peak, $W$ is the width (FWHM), $M$ is the length of the DNA fragment (nt), and $M_2 > M_1$. A value of $R \geq 0.5$ is the minimum resolution for single-base resolution of sequencing fragments with no additional advanced data manipulation [32]. Resolution was also plotted versus electric field strength in Fig. 2A, demonstrating a major advantage of FSCE separations over conventional polymer matrix-based separations. When DNA is separated in a sieving polymer at increasing $E$, separation resolution starts to degrade [33]. However, Fig. 2A clearly shows that resolution does not decrease with increased $E$, but in fact remains constant. The ability to separate DNA at increased $E$ without losing resolution is a significant advantage since analysis time can be drastically decreased by increasing $E$.

FSCE theory predicts the ability to increase $E$ without loss of resolution and this is, to the best of our knowledge, the first proof of this phenomenon beyond $E = 319$ V/cm [21]. Resolution between peaks is essentially a ratio of peak spacing to peak width. In FSCE, peak spacing decreases more slowly than peak width with increased $E$. In an ideal, diffusion-limited case, peak width (in seconds) will decrease with $E^{-1.5}$, and peak spacing (in seconds) will decrease with $E^{-1}$ [24]. Peak width and peak spacing for the separations in Fig. 1 are plotted versus $E$ (Fig. 2B). Experimentally, peak spacing decreases with $E^{-1}$, but peak width decreases slower than predicted ($\sim E^{-1.2}$), indicating the presence of band broadening from other sources.

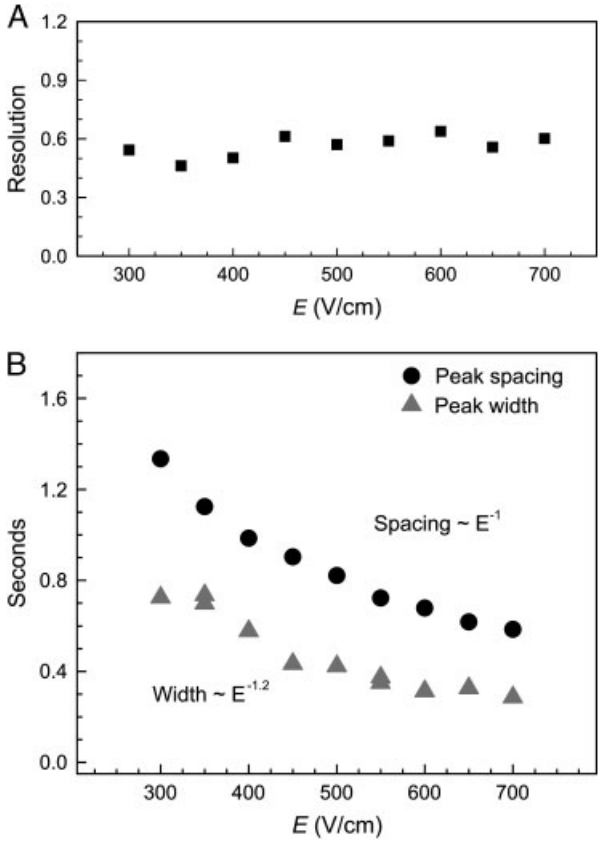


**Figure 2.** Peak analysis of the separations in Fig. 1. (A). Resolution between the peaks, plotted versus electric field strength $E$. (B). The spacing between peaks (black circles) and the width of peaks (grey triangles) from Fig. 1 are measured in seconds and plotted versus $E$.

### 3.3 Band broadening during free-solution separations on microchips

An analysis of plate height, $H$, will help determine the sources of band broadening that caused peak width in Fig. 1 to decrease more slowly than expected in an ideal case. The band broadening sources, which assume negligible Joule heating based on dissipation of thermal gradients by the large thermal mass of the glass microchip (J. I. Mohlo, Stanford University 2001), are described with this equation for theoretical plate height, $H$ [22, 25]:

$$H = \frac{A}{L} + \frac{2D}{u} + Wu + BL \quad (2)$$

The four possible sources of band broadening are depicted by Eq. (2) in this order: (i) injection plug width, (ii) thermal diffusion, (iii) analyte–wall interactions, and (iv) drag-tag polydispersity; $A$, $W$ and $B$ are constants related to i, iii, and iv, respectively, $D$ is diffusion coefficient, $L$ is separation length (inlet-to-detector), and $u$ is electrophoretic velocity ($u = \mu E = T/L$). Assuming a Gaussian profile, the plate height, $H$, is determined from the raw data:

$$H = \frac{\sigma_x^2}{L} = \frac{w^2 u^2}{L \cdot 8\ln(2)} \quad (3)$$

where $\sigma_x^2$ is spatial peak variance and is related to temporal peak variance $\sigma^2$ ($\sigma^2 = \sigma_x^2/u^2$), which is related to temporal peak width $w$ [$w^2 = \sigma^2 8\ln(2)$].

By varying $L$ and $u$, two sets of experiments can independently examine all four possible causes of band broadening. The separation channel length, $L$, was varied by moving the focused laser spot from the maximum of $L = 7.2$ cm to a minimum of $L = 0.8$ cm (in 0.8-cm increments). This data determined if injection plug width and drag-tag polydispersity were major contributors to peak broadness. To control velocity, $u$, the applied separation voltage was varied from 1700–5950 V ($E = 200$–$700$ V/cm, increased in 50-V/cm increments). This determined if thermal diffusion and analyte–wall interactions were major contributors to band broadening. Representative electropherograms from the length and velocity (voltage) series are shown in Fig. 3 for the 18-mer and 27-mer protein drag-tags. A 74-nt DNA oligomer with a 5′-thiol modification and internal fluorescein was used as the test DNA molecule. Previous studies of $H$ in FSCE separations used DNA fragments with lengths $\sim$ 60–110 nt, thus the choice of a 74-nt fragment follows precedent [22, 25, 26].

 

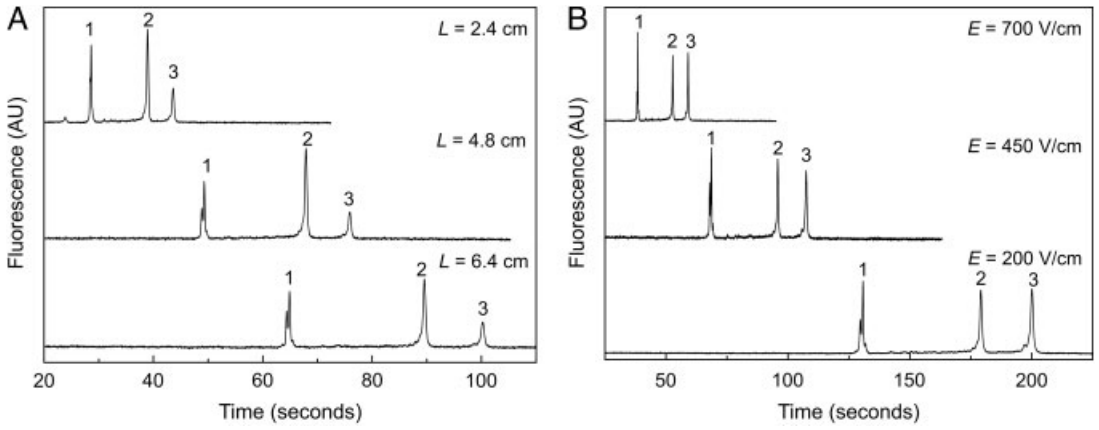


**Figure 3.** Representative separations of drag-tagged DNA at varied separation channel length (A) and applied voltage (B). Peak 1 is the ''free'' ssDNA (74 nt). Peaks 2 and 3 are the 74 nt ssDNA conjugated to the 18-mer (141-aa, peak 2) and 27-mer (204-aa, peak 3) drag-tags. Separations performed using the same conditions as Fig. 1, except the length series (A) was at $E = 350$ V/cm and a separation channel of $L = 0.8$–$7.2$ cm and the velocity series (B) was at $L = 7.2$ cm and an applied voltage of 1700–5950 V ($E = 200$–$700$ V/cm).

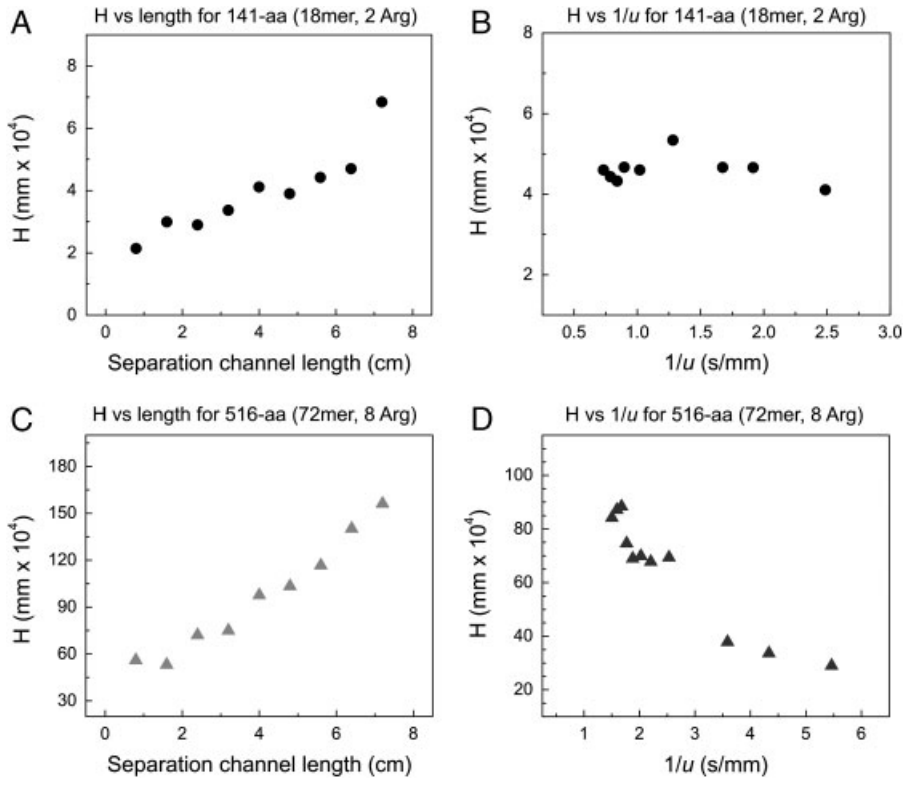


**Figure 4.** Graphs of plate height $H$ versus $L$ (A, C) and $H$ versus $1/u$ (B, D) for separations with the 74-nt DNA conjugated to the 18-mer (141-aa, black circles, A, B) and 72-mer (516-aa, grey triangles, C, D) drag-tags. Separation conditions are the same as Fig. 3, $n = 1$.

The separation channel length, $L$, and velocity, $u$, series were first performed with four drag-tags from the same family. Drag-tags with 18, 27, 36, and 72 repeats of the seven amino acid ''monomer'' (GAGTGSA) conjugated to the 74-nt oligomer were separated under all the test conditions (J. S. Lin et al., paper submitted) [26]. As a reminder, the amino acid sequence of these protein polymers was mutated by *E. coli* such that 1 of every 9 serine residues is a positively charged arginine. Plate height $H$ was calculated for each separation, and the results are plotted in Fig. 4 (18-mer and 72-mer) and Supporting Information Fig. S-3 (27-mer and 36-mer). Contributions to band broadening from injection plug width and drag-tag polydispersity are decoupled in the plot of $H$ versus $L$. If $H(L) \sim 1/L$, band width is due to injection plug width. If $H(L) \sim L$, then drag-tag polydispersity is a major contributing factor. $H$ is plotted versus $1/u$ to examine the effects of thermal diffusion and interactions between the drag-tag and microchannel walls. If

 

**Table 1.** Summary of plate height, *H*, from Fig. 4 and S-3; the dominant contributing factors to band broadening in separations with each drag-tag are denoted by an X

| Drag-tag | Injection plug width | Drag-tag polydispersity | Analyte–wall interactions | Thermal diffusion |
|---|---|---|---|---|
| 18mer (141-aa, 2 Arg) | – | X | – | – |
| 27mer (204-aa, 3 Arg) | – | X | – | – |
| 36mer (267-aa, 4 Arg) | – | X | X | – |
| 72mer (516-aa, 8 Arg) | – | X | X | – |

$H(1/u) \sim 1/u$, thermal diffusion is a dominant factor; if $H(1/u) \sim u$, then analyte–wall interactions are causing increased band width.

For all drag-tags, the graph of $H$ versus $L$ shows $H$ increasing with separation channel length (Fig. 4 and Supporting Information Fig. S-3), indicating that protein polymer polydispersity is a major contributing factor to band broadening in separations with this entire family of drag-tags. The values of $H$ shown in the $H$ versus $1/u$ plots remain steady for the 18-mer and 27-mer (Fig. 4 and Supporting Information Fig. S-3), indicating that neither thermal diffusion nor interactions between drag-tags and microchip walls are causing increased band width. However, the graphs of $H$ versus $1/u$ for the 36-mer and 72-mer proteins show increased $H$ at decreased $1/u$ (Supporting Information Figs. S-3 and 4), indicating that the increased length and cationic quality of the two larger proteins allowed analyte–wall interactions to become a contributing factor to increased peak width. These findings are summarized in Table 1. For the two ''highly'' charged drag-tags, interactions between the DNA–drag-tag conjugate and the microchip walls were the main contributing factor to band broadening (Supporting Information Fig. S-5 and Supporting Information Table S-1) despite the robust pHEA wall coating, confirming the finding that protein drag-tags with $>3$ positively charged amino acids experience peak broadness due to analyte–wall interactions.

## 4 Concluding remarks

Free-solution electrophoretic separations of ssDNA coupled to protein polymer drag-tags were performed in a microfluidic device. The typical conditions for microchip separations of DNA in a sieving polymer were reoptimized for free-solution separations. Buffer ionic strength was increased to achieve maximum friction from the drag-tag, and a new combination heating-plate/chip-caddy significantly increased well volume. To minimize peak tailing and achieve Gaussian-shaped peaks, separations were performed using a simple-cross injection geometry and constant ''pullback'' voltage.

The efficiency of FSCE separations in microchips using protein polymer drag-tags was tested by determining resolution between two lengths of DNA conjugated to identical protein drag-tags. The fragments were separated at increasing electric field strength, starting at a comparable value to CE and incrementally moving toward the highest possible $E$ (700 V/cm) for our system, which is greater than twice the $E$ of CE separations. Contrary to polymer-based separations, no loss of resolution occurs with increased $E$; the resolution remained constant. Theoretically, no loss of resolution is expected since peak spacing is predicted to decrease slower than peak width when $E$ is increased. To the best of our knowledge, this is the first proof of that theory beyond $E = 319$ V/cm. Experimentally, peak width decreased slower than predicted, and a thorough investigation determined the major sources of band broadening when protein polymer drag-tags are used to separate FSCE samples on glass microchips. For all four protein polymers with the monomer unit GAGTGSA, polydispersity of the drag-tag was the significant contributor to peak broadening. As the length of the protein increased, so did the number of positively charged arginines, and separations with the two largest proteins (36-mer and 72-mer) also saw increased peak width due to interactions with the microchannel walls, despite using a dynamic wall coating. Two ''highly'' charged protein polymer drag-tags were also tested, and analyte–wall interactions were found to be a significant contributor to in band broadening. While cationic residues do increase hydrodynamic drag without adding length, this study shows that once the number of positively charged amino acids increases beyond 3, interactions between microchannel walls and drag-tags cause peak degradation.

Overall, this study is a significant step forward for FSCE separations on microfluidic devices. Previously, only one separation had been achieved using the smallest protein drag-tag (18-mer). This study shows efficient injections and separations with even the longest protein drag-tags (516-aa), which is the drag-tag expected to enable sequencing of 400 bases [26]. Experimental results showing no loss of resolution at increased $E$, up to the maximum of the HVPS, indicate that the speed of free-solution sequencing separations will be able to be pushed to the shortest possible time while still achieving single-base resolution (if not beyond the speed of the detector). Based on the previous reduction in analysis time of the SBE-FSCE genotyping separation on microchips, we expect that we may be able to sequence at least 250 bases in under 3 min [26, 28]. Future work on sample purification and concentration will be necessary in order to transition FSCE sequencing separations onto microfluidic devices.

 

*This work was supported by National Institutes of Health grants (NHGRI Grants 5R01HG002918-04, 5R01HG001970-09, and 1RC2HG005596-01) and a National Science Foundation Graduate Research Fellowship for J. C. A.*

*The authors have declared no conflict of interest.*

## 5 References

[1] Lander, E. S., Linton, L. M., Birren, B., Nusbaum, C., Zody, M. C., Baldwin, J., Devon, K., Dewar, K. et al., *Nature* 2001, *409*, 860–921.

[2] Venter, J. C., Adams, M. D., Myers, E. W., Li, P. W., Mural, R. J., Sutton, G. G., Smith, H. O., Yandell, M. et al., *Science* 2001, *291*, 1304–1351.

[3] Hert, D. G., Fredlake, C. P., Barron, A. E., *Electrophoresis* 2008, *29*, 4618–4626.

[4] Manz, A., Harrison, D. J., Verpoorte, E. M. J., Fettinger, J. C., Paulus, A., Ludi, H., Widmer, H. M., *J. Chromatogr.* 1992, *593*, 253–258.

[5] Harrison, D. J., Manz, A., Fan, Z. H., Ludi, H., Widmer, H. M., *Anal. Chem.* 1992, *64*, 1926–1932.

[6] Fredlake, C. P., Hert, D. G., Root, B. E., Barron, A. E., *Electrophoresis* 2008, *29*, 4652–4662.

[7] Emrich, C. A., Tian, H., Medintz, I. L., Mathies, R. A., *Anal. Chem.* 2002, *74*, 5076–5083.

[8] Martynova, L., Locascio, L. E., Gaitan, M., Kramer, G. W., Christensen, R. G., MacCrehan, W. A., *Anal. Chem.* 1997, *69*, 4783–4789.

[9] Obubuafo, A., Balamurugan, S., Shadpour, H., Spivak, D., McCarley, R. L., Soper, S. A., *Electrophoresis* 2008, *29*, 3436–3445.

[10] Shadpour, H., Hupert, M. L., Patterson, D., Liu, C., Galloway, M., Stryjewski, W., Goettert, J., Soper, S. A., *Anal. Chem.* 2007, *79*, 870–878.

[11] Liu, Y., Ganser, D., Schneider, A., Liu, R., Grodzinski, P., Kroutchinina, N., *Anal. Chem.* 2001, *73*, 4196–4201.

[12] McDonald, J. C., Duffy, D. C., Anderson, J. R., Chiu, D. T., Olivier, H. W., Schueller, J. A., Whitesides, G. M., *Electrophoresis* 2000, *21*, 27–40.

[13] Toepke, M. W., Beebe, D. J., *Lab Chip* 2006, *6*, 1484–1486.

[14] Bienvenue, J. M., Legendre, L. A., Ferrance, J. P., Landers, J. P., *Forensic Sci. Int.-Genet.* 2010, *4*, 178–186.

[15] Easley, C. J. K., Bienvenue, J. M., Legendre, L. A., Roper, M. G., Feldman, S. H., Hughes, M. A., Hewlett, E. L., Merkel, T. J., Ferrance, J. P., Landers, J. P., *Proc. Natl. Acad. Sci. USA* 2006, *103*, 19272–19277.

[16] Hopwood, A. J., Hurth, C., Yang, J. N., Cai, Z., Moran, N., Lee-Edghill, J. G., Nordquist, A., Lenigk, R., Estes, M. D., Haley, J. P., McAlister, C. R., Chen, X., Brooks, C., Smith, S., Elliott, K., Koumi, P., Zenhausern, F., Tully, G., *Anal. Chem.* 2010, *82*, 6991–6999.

[17] Blazej, R. G., Kumaresan, P., Mathies, R. A., *Proc. Natl. Acad. Sci. USA* 2006, *103*, 7240–7245.

[18] Fredlake, C. P., Hert, D. G., Kan, C. W., Chiesl, T. N., Root, B. E., Forster, R. E., Barron, A. E., *Proc. Natl. Acad. Sci. USA* 2008, *105*, 476–481.

[19] Albarghouthi, M. N., Stein, T. M., Barron, A. E., *Electrophoresis* 2003, *24*, 1166–1175.

[20] Mayer, P., Slater, G. W., Drouin, G., *Anal. Chem.* 1994, *66*, 1777–1780.

[21] Heller, C., Slater, G. W., Mayer, P., Dovichi, N., Pinto, D., Viovy, J. L., Drouin, G., *J. Chromatogr. A* 1998, *806*, 113–121.

[22] Ren, H., Karger, A. E., Oaks, F., Menchen, S., Slater, G. W., Drouin, G., *Electrophoresis* 1999, *20*, 2501–2509.

[23] Vreeland, W. N., Desruisseaux, C., Karger, A. E., Drouin, G., Slater, G. W., Barron, A. E., *Anal. Chem.* 2001, *73*, 1795–1803.

[24] Meagher, R. J., Won, J. I., McCormick, L. C., Nedelcu, S., Bertrand, M. M., Bertram, J. L., Drouin, G., Barron, A. E., Slater, G. W., *Electrophoresis* 2005, *26*, 331–350.

[25] Meagher, R. J., Won, J. I., Coyne, J. A., Lin, J., Barron, A. E., *Anal. Chem.* 2008, *80*, 2842–2848.

[26] Albrecht, J. C., Lin, J. S., Barron, A. E., *Anal. Chem.* 2011, *83*, 509–515.

[27] Sinville, R., Coyne, J., Meagher, R. J., Cheng, Y. W., Barany, F., Barron, A., Soper, S. A., *Electrophoresis* 2008, *29*, 4751–4760.

[28] Meagher, R. J., Coyne, J. A., Hestekin, C. N., Chiesl, T. N., Haynes, R. D., Won, J. I., Barron, A. E., *Anal. Chem.* 2007, *79*, 1848–1854.

[29] Won, J. I., Barron, A. E., *Macromolecules* 2002, *35*, 8281–8287.

[30] Chiesl, T. N., Shi, W., Barron, A. E., *Anal. Chem.* 2005, *77*, 772–779.

[31] Shi, Y. N., Anderson, R. C., *Electrophoresis* 2003, *24*, 3371–3377.

[32] Best, N., Arriaga, E., Chen, D. Y., Dovichi, N. J., *Anal. Chem.* 1994, *66*, 4063–4067.

[33] Heller, C., *Electrophoresis* 1999, *20*, 1978–1986.

 